Engineered Science
DOI: https://dx.doi.org/10.30919/es1077

Photocatalytic Degradation of Rose Bengal Dye using Chemically Synthesized Pristine and Molybdenum doped Zinc Oxide

Vishal Kadam,[1] Chaitali Jagtap,[1] Vilas Kumkale,[1] Udayabhaskar Rednam,[2] Prasad Lokhande[1, 2,*] and Habib Pathan[1,*]

Abstract

In this comprehensive study, the synthesis of pure zinc oxide (ZnO) nanoparticles and their molybdenum-doped counterparts (Mo: ZnO) was meticulously carried out through a refined reflux chemical process. The doping concentrations were carefully controlled at 5 and 10% wt%, aiming to investigate the impact on the nanoparticles' properties. A suite of characterization techniques was employed to delve into the structural, morphological, optical, and photocatalytic nuances of the synthesized materials. The crystalline nature and particle size variations were revealed through X-ray diffraction (XRD) analysis, which indicated a discernible decrease in ZnO crystallite size with an increase in Mo doping levels. Scanning electron microscopy (SEM) provided insights into the morphology, displaying a transition from irregular spherical shapes in pure ZnO to a more uniform morphology upon Mo incorporation. Elemental mapping and energy-dispersive X-ray spectroscopy (EDX) analyses corroborated the elemental composition, confirming the integration of Zn, O, and Mo within the samples. Optical properties were probed using UV-Visible spectroscopy, which demonstrated an enhancement in absorption capabilities and modulation of the band gap as a function of Mo doping; the band gap narrowed progressively from 2.9 to 3.14 eV with increasing Mo content from 0 to 10 wt%. Photocatalytic performance was quantitatively assessed, revealing that Mo-doped ZnO nanoparticles exhibited superior activity compared to their undoped counterparts. Notably, the sample with 5% Mo doping achieved an impressive 91% decolorization of dye, signifying a potent photocatalytic effect. This heightened activity was further evidenced by a minimal half-life and a rate constant for the 5 wt% Mo-doped sample that was twice as high as that of pure ZnO, underscoring the significant enhancement brought forth by molybdenum doping.

Keywords: Photocatalytic degradation; Molybdenum; Doping; Rose Bengal.
Received: 31 October 2023; Revised: 05 December 2023; Accepted: 05 December 2023.
Article type: Research article.

1. Introduction

One of the significant challenges the entire world is currently facing is water pollution. This includes wastewater from industries such as textiles and other dye-producing sectors, which impacts not only humans but also the environment.[1–3] Persistent and non-biodegradable organic compounds are often the culprits behind pollution, adversely affecting both living entities and inanimate objects.[4–6] The recycling and treatment of wastewater are garnering significant interest. Within this framework, it is essential to conduct further research into cost-effective and eco-friendly water purification techniques.[7–9] Toxic substances from industrial wastewater have been reported to be removed using a variety of techniques, including ultrafiltration,[10] reverse osmosis,[11] adsorption on different materials such as activated carbon,[12] wood chips,[13] and silica gel.[14] Two critical drawbacks of the indicated procedures are the transformation of the aqueous phase into a stable network, which leads to secondary pollution, and the requirement for multiple purification processes that are costly and time-consuming.[15] Heterogeneous photocatalysis is one of several modern methods extensively used for dye degradation.[16] In the process of photocatalysis, light energy is absorbed by a semiconducting material, which excites the electrons to move from the valence band to the conduction band. The valence band in this case generates holes, while the conduction band generates electrons.[17] In recent days, a great deal of interest generated in the degradation of organic

[1] *Advanced Physics Laboratory, Department of Physics, Savitribai Phule Pune University, Pune, 411007, India.*
[2] *Departamento de Mecánica, Facultad de Ingeniería, Universidad Tecnológica Metropolitana, Santiago 8330383, Chile.*
**Email:* p.eknath@utem.cl (P. E. Lokhande), pathan@physics.unipune.ac.in (H. M. Pathan)

contaminants in water by utilizing a semiconductor as a photocatalyst.[18]

Scientists have primarily focused on semiconductor photocatalysts to tackle environmental issues. To date, a variety of semiconductor photocatalysts have been developed, including TiO_2, ZnO, SnO_2, Cu_2O, CdS, WO_3, $C3N_4$, and others.[19–22] Among them, ZnO is a well-known semiconductor with a large band gap of 3.37 eV and is appealing to the development of innovative ultraviolet lasers, nanogenerators, solar cells, chemical and biological sensors, and so on.[23] Because ZnO and TiO_2 have similar bandgaps, numerous researchers attempted to substitute costly TiO_2 photocatalysts with ZnO photocatalysts.[24] Due to the photosensitivity, high oxidizing properties, non-toxicity, favourable exciton binding energy (60 MeV), and outstanding chemical and mechanical stability, ZnO is one of the most popular semiconductors utilized as an excellent material for the photocatalytic process.[18] The photogenerated electrons and holes subsequently move to the ZnO surface, where they produce highly reactive oxygen species (ROS) such as superoxide anion ($O_2^{\bullet -}$) and hydroxyl radical ($^{\bullet}OH$).[25] The quick recombination rate of photogenerated electron-hole pairs[26] resulting in low quantum efficiency and significantly reduced photocatalytic activity is one of the key drawbacks of pure ZnO nanoparticles.[25] It is possible to increase the photocatalytic activity of ZnO by doping transition metal ions into its crystal structure. This is done by creating new energy levels in the band gap, which principally increase the charge separation efficiency of e^-/h^+ by defining electron traps.[26] Co, Mn, Fe, Cr, Cu, Al, Sn, Sr, and non-metallic elements including N, S, and P have been investigated as doping elements to boost the photocatalytic effectiveness of ZnO, *i.e.*, decrease the bandgap and recombination rate.[15] Jagtap *et al.* demonstrated tin-doped ZnO for photocatalytic activity to reduce environmental pollutants.[27] Shah *et al.* synthesized copper-doped ZnO nanorods for efficient photodegradation of methylene blue and methyl orange and found an efficiency of 57.5% and 60% respectively for a time of 180 minutes.[28]

In the present study, we have synthesized bare ZnO and Mo-doped ZnO nanoparticles using a practical combustion synthesis technique. The synthesized samples were characterized using various advanced techniques to analyse their properties. The fabricated samples of bare ZnO and Mo-doped ZnO were tested for their potential as photocatalysts for water purification. From obtained results show that doping of Mo enhances the efficiency of ZnO.

2. Materials and methods

Zinc acetate dehydrate [Zn $(CH_3COOH)_2{\cdot}2H_2O$], Sodium Molybdate [Na_2MoO_4], Sodium Hydroxide (Sisco Research Lab (SRL)), Diethylene glycol (HPLC), Rose Bengal dye (Himedia Laboratories), Citric Acid Monohydrate (Sisco Research Lab (SRL)), and Double Distilled water (DDW).

2.2 Synthesis of ZnO and Mo-doped ZnO nanoparticles

For the synthesis of ZnO simple and easy, the reflux method was used and the process was explained as follows. To prepare a homogeneous solution, 0.1 M zinc acetate dehydrate ($Zn(CH_3COOH)_2{\cdot}2H_2O$) dissolved in a single distilled water solution. Then, 0.2 M citric acid was added to the above solution and continuously stirred for 20 min, and then added HCl to obtain a clear solution. The reflux process was conducted at 120 °C, and a dropwise solution of sodium hydroxide (2M) was added to the solution without disturbing the stirring process. The sodium hydroxide was added in its entirety, resulting in a milky, white precipitate. The solution was left to cool overnight. Subsequently, the precipitate was centrifuged multiple times at a rate of 3750 rpm with a mixture of water and acetone, and the powder was dried in an incubator before being annealed at a temperature of 450 °C for one hour. A similar reflux system was carried out for Molybdenum doping in ZnO. 0.1 M zinc acetate dehydrate ($Zn(CH_3COOH)_2{\cdot}2H_2O$) dissolved in a single distilled water solution. Then, 0.2 M citric acid was added to the above solution and continuously stirred for 20 min, and then added HCl to obtain a clear solution. The reflux process was conducted at 120 °C, and then 5, 10 wt% Sodium Molybdate solution was added to the above solution. After that process dropwise, a solution of sodium hydroxide (2M) was added to the solution without disturbing the stirring process. The sodium hydroxide was added in its entirety, resulting in a milky, white precipitate. The solution was left to cool overnight. Subsequently, the precipitate was centrifuged multiple times at a rate of 3750 rpm with a mixture of water and acetone, and the powder was dried in an incubator before being annealed at a temperature of 450 °C for one hour.

2.3 Characterization methods

The samples were examined using various methods of characterization to acquire the structural, morphologic, and optical properties necessary for the photocatalytic process. The structural analysis of the samples was carried out using the X-ray diffraction (XRD) technique (model: XRD, Rigaku "D/B max-2400", Cu Kα = 0.154 nm) in the scanning angle (2θ) from 20 - 80. The microstructural properties of the samples such as morphology and elemental composition were determined using a high-resolution (model: JEOL-JSM 6360-A) scanning electron microscope (SEM) equipped with

energy-dispersive X-ray analysis (EDX). The optical absorption spectra of the nanoparticles were recorded using a UV–VIS spectrophotometer (model: JASCO V-670). In the photo-catalytical experiments, the synthesized zinc oxide (ZnO) and molybdenum (5% and 10%) doped zinc oxide nanoparticles were exposed to ultraviolet (UV) light (visible Osramm 300 Watt \) to remove the Rose Bengal colour. Decolorization efficiency was calculated.

3. Results and discussion

3.1 Structural properties

Figure 1 shows the peaks obtained for XRD analysis of a sample of pure ZnO and 5% Mo: ZnO and 10% Mo: ZnO. All samples exhibited the diffraction peaks at 2θ angle of 31.78°, 34.42°, 36.26°, 42.58°,56.62°,62.82°,67.94°, and 69.08° corresponding to the crystal planes (100), (002), (101), (102), (110), (103), (112), and (101) respectively of the hexagonal structure of wurtzite structure, as specified by the (JCPDS) 36-1451.[18,29] When Mo was present, the peak was most commonly observed along the plane of (101) and the interplanar space (d_{101}). The d_{101} values of ZnO, Mo (5 wt%), and Mo (10 wt%) were 0.246, 0.247, and 0.246 nm respectively. The d_{101} values indicated slight variations in peak intensity. This suggests that the Mo ion is incorporated into the lattice of ZnO at the substitutional or interstitial sites, which may affect the crystalline resolution of the samples.[23] There is no indication of the Mo peaks denoting the absence of the secondary phase impurities. The ionic radii of ZnO in Zn^{2+} and O^{2-} are 0.074 nm and respectively 0.14 nm respectively.[29] The condition of diffraction is the Bragg's law given by,

$$2dsin\theta = n\lambda \quad (1)$$

where d denotes inter-planer spacing, θ denotes incident angle, λ denotes X-ray wavelength, and n denotes diffraction order.[30] Tables 1, 2 and 3 show the Crystal size, Interplanar Distance, and Peak Intensity of Pure ZnO, 5% Mo: ZnO and 10% Mo: ZnO. Bare ZnO has an interplanar spacing index of approximately 0.246 nm (d_{101}) and is indexed to hexagonal Wurtzite. However, when doping ions are added to the lattice of ZnO, interplanar spacing changes. These changes indicate that the doping ions have been successfully incorporated into the lattice side of ZnO. The powder has a good crystallinity due to its higher intensity and narrower peaks. The crystalline sizes of the Mo-doped ZnO were determined utilizing an X-ray line-broadening method using the Scherrer equation,[31]

$$D = \frac{k\lambda}{\beta cos\theta} \quad (2)$$

where D denotes crystallite size, θ denotes incident angle, λ denotes wavelength of x-rays, and β denotes full width at half maxima (FWHM). Table 4 tabulates Lattice parameters and volume of the unit cell with theoretical Pure ZnO and Mo-doped ZnO.

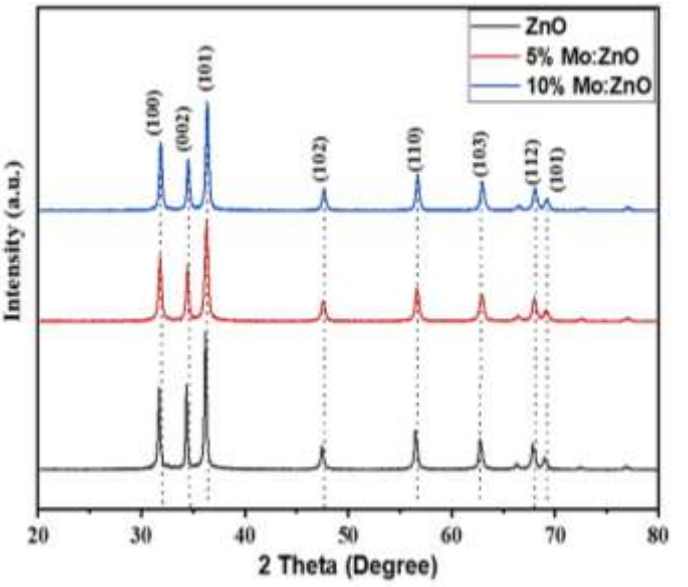

Fig. 1 The X-ray diffraction patterns of pure, 5% and 10% Mo-doped ZnO nanoparticles.

The XRD pattern was submitted to Rietveld refinement to analyse the X-ray diffraction pattern of polycrystalline material which studies the parameters such as crystal structure, microstructure, and phase composition[32,33] Fig. 2 shows Rietveld refinement of pure ZnO, 5% Mo-doped ZnO, and 10% Mo-doped ZnO nanoparticles. The Rietveld-based method determines the phase abundance and has the potential to produce more accurate and precise results than those obtained from single-peak methods. Various crystallographic terms such as space group, lattice parameters, temperature factors, and atom position. The calculated pattern is based on a model that includes the crystal structure of every phase present in the material. Here in the figure, red indicates the observed intensity of the diffraction peaks Green lines indicate the differences between observed and calculated intensity. For a clear study, the baseline is created with a solid black line that indicates observed and calculated intensities. Various parameters such as Rwp, Rexp, and goodness of Fit (GoF) are calculated using Rietveld refinement. All the parameters are discussed in the Table 1. Rietveld refinement also confirms the doping of Mo in ZnO nanoparticles. The grain size is found to be minimum for 5% Mo-doped ZnO nanoparticles.

3.2 Optical Properties: UV-visible absorbance spectra

Figure 3 shows the UV-visible absorption spectra of Mo-doped ZnO samples prepared with Zinc Acetate precursor showing a significant absorption edge for ZnO in the UV range of 200–420 nm. The Energy Bandgap (E_g) is calculated by

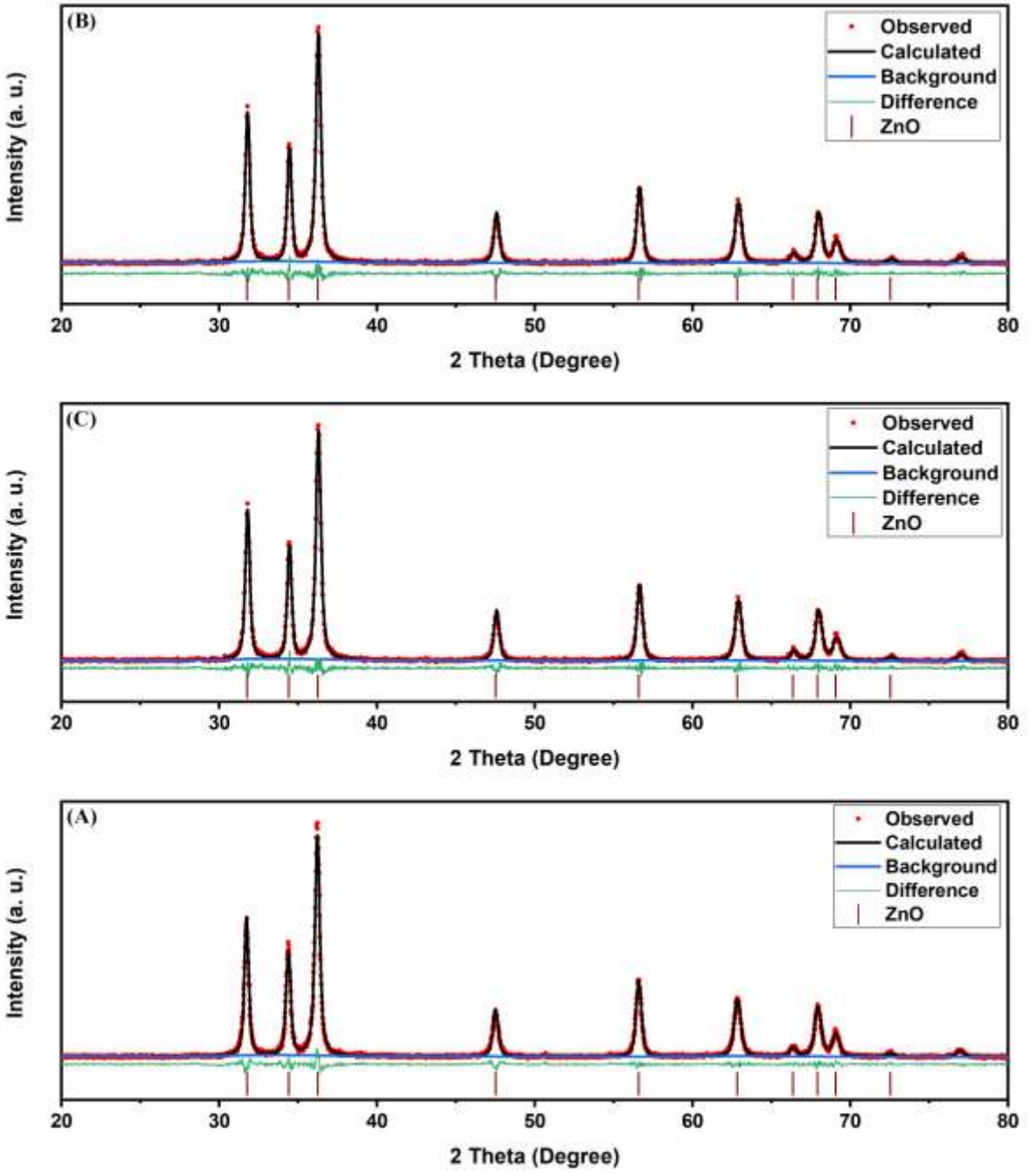

Fig. 2 Rietveld refinement of pure, 5% and 10% Mo-doped ZnO nanoparticles.

Table 1. Average Crystal Size, Interplanar Distance, and Peak Intensity of Pure ZnO, D=27 nm.

Sr.	2Θ		{hkl}	Intensity (%)		d (Å)		Crystallite size
No.	Theoretical	Experimental	planes	Theoretical	Experimental	Theoretical	Experimental	D (nm)
1	31.77	31.82	100	57	62.76	2.81	2.80	31.85
2	34.42	34.48	002	44	54.27	2.60	2.60	37
3	36.25	36.34	101	100	100	2.47	2.46	30.65
4	47.53	47.64	102	23	19.01	1.91	1.90	25.7
5	56.603	56.72	110	32	35.12	1.62	1.62	26.57
6	62.864	62.94	103	29	25.68	1.477	1.47	23.56
7	66.38	66.6	200	4	3.92	1.407	1.4	23.7
8	67.963	68.02	112	23	22.22	1.378	1.37	21.72
9	69.1	69.14	201	11	10	1.35	1.35	20.61

Table 2. Average Crystal Size, Interplanar Distance, and Peak Intensity of 5% Mo: ZnO, D=22 nm.

Sr.	2Θ		{hkl}	Intensity (%)		d (Å)		Crystallite size
No.	Theoretical	Experimental	planes	Theoretical	Experimental	Theoretical	Experimental	D (nm)
1	31.768	31.8	100	57.8	63.64	2.81451	2.81	25.7
2	34.422	34.46	002	41.9	52.32	2.60329	2.6	29.7
3	36.253	36.28	101	100	100	2.47592	2.47	24.47
4	47.539	47.54	102	21.4	21.99	1.91112	1.9	20.85
5	56.594	56.62	110	30.3	37.23	1.62496	1.62	22.61
6	62.858	62.9	103	26.5	28.79	1.47725	1.47	21.15
7	66.374	66.38	200	4	3.42	1.40726	1.4	23.61
8	67.947	67.98	112	21.3	23.3	1.37846	1.37	18.47
9	69.085	69.12	201	10.2	11.24	1.35851	1.35	18.42

Table 3. Average Crystal Size, Interplanar Distance, and Peak Intensity of 10% Mo: ZnO, D=24 nm.

Sr.	2Θ		{hkl}	Intensity (%)		d (Å)		Crystallite size
No.	Theoretical	Experimental	planes	Theoretical	Experimental	Theoretical	Experimental	D (nm)
1	31.84	31.86	100	56.2	63.87	2.8082	2.8	30.4
2	34.503	34.5	002	41.2	46.04	2.5974	2.6	30.29
3	36.337	36.34	101	100	100	2.4703	2.46	28.27
4	47.653	47.66	102	21.5	20.91	1.9068	1.9	24.13
5	56.731	56.72	110	30.9	34.45	1.6213	1.62	25.15
6	63.016	62.98	103	27.2	26.02	1.4739	1.47	22.32
7	66.541	66.48	200	4.1	6.32	1.4041	1.4	21.29
8	68.12	68.06	112	22.7	18.74	1.3753	1.37	20.52
9	69.261	69.24	201	11.2	13.47	1.3554	1.35	19.74

Table 4. Lattice parameters, Volume of the unit cell with theoretical Pure ZnO and Mo-doped ZnO.

Compound	Lattice Parameter (Å)		Volume of Unit Cell (Å)	
	Theoretical	Experimental	Theoretical	Experimental
ZnO	a=b= 3.25 c= 5.21	a=b= 3.24 c= 5.20	47.62	47.27
Mo: ZnO 5%	a=b= 3.25 c= 5.20	a=b= 3.24 c= 5.20	47.62	47.27
Mo: ZnO 10%	a=b= 3.25 c= 5.19	a=b= 3.24 c= 5.20	47.88	47.27

plotting the $(Absorbance)^2$ vs. Photon Energy (hν) graph for both pure and Mo-doped ZnO samples. Significant changes in band gap energy were observed in the range of 2.9–3.2 eV after doping. It is also observed that an increase in the concentration of Mo ions results in significant changes in the absorption spectra for ZnO showing the surface plasma band as a large bulge across the visible area resulting in high absorbance across the entire visible area with high Mo concentration.[16,34] As expected, the incorporation of dopants into the ZnO lattice shifted the fundamental absorption edge towards the longer wavelength *i.e.* redshift, which decreases the band gap energy. As predicted, the addition of dopants to the zinc oxide (ZnO) lattice caused the basic absorption edge to shift to the longer wavelength, redshift, resulting in a decrease in band gap energy. As predicted, the addition of dopants to the lattice of ZnO shifted the basic absorption edge toward the longer wavelength, or blueshift, increasing band gap energy.

3.3 Morphological study

SEM is one of the effective methods for determining the surface structure, morphology, and size of nanoparticles. In Fig. 4, the prepared samples are SEM analysed to see how Mo dopants affect the surface structure of ZnO. The sample of pure ZnO shows non-convex spherical-shaped nano-clusters with agglomerated morphology. The SEM micrographs reveal a pattern of agglomeration and non-uniform particle sizes. As the Mo doping concentration rises, the agglomeration increases, which may be caused by the formation of Mo: ZnO nanoparticles. Additionally, the particle sizes also vary with the Mo doping concentration.[35] As the concentration of Mo dopants increases in the ZnO, the structure of the molecules breaks down and forms tiny, round particles. We may also observe an increase in the particle size of Mo: ZnO NP

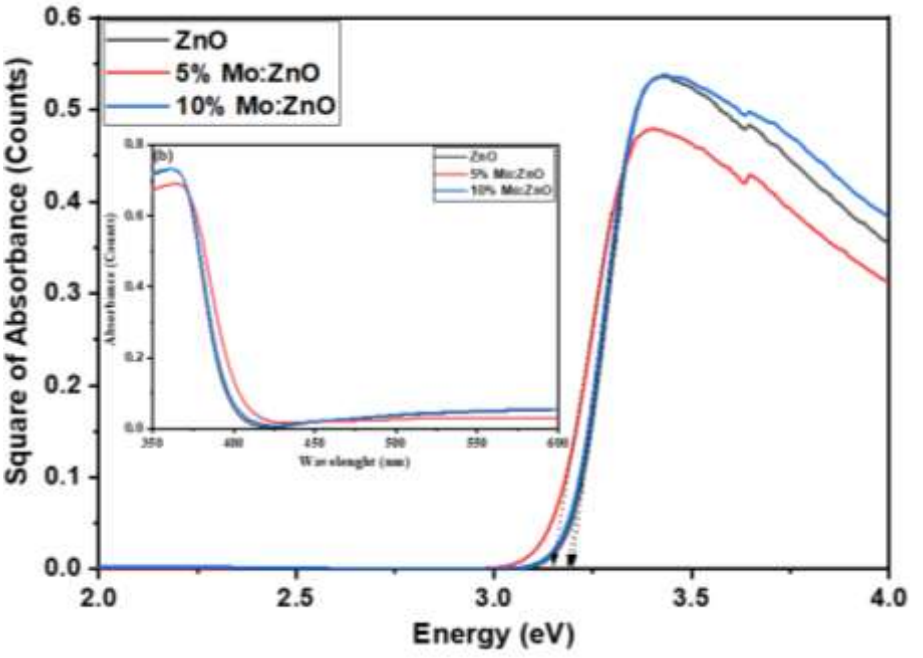

Fig. 3 Tauc plot [(absorbance)^2 vs photon energy (hν)] for bare ZnO and Mo doped ZnO (5 and 10 %) (Inside) UV-vis absorbance spectra of bare ZnO and Mo doped ZnO (5 and 10 %).

samples, which may enhance their absorption properties. The growth of NPs may be due to increased energy release, resulting in rapid growth.[36] In the full SEM images, you can see the spherical particles with clearly defined edges/ boundaries and average sizes. The grain size is around 35-38 nm, which is calculated with ImageJ software and is in line with the analysis of XRD data in terms of Scherrer's formula.[29]

3.4 Compositional analysis

The energy dispersion spectroscopy mapping (EDS mapping) examined the arrangement and distribution of the atoms present in the Mo-doped ZnO nanoparticles. Fig. 5 illustrates

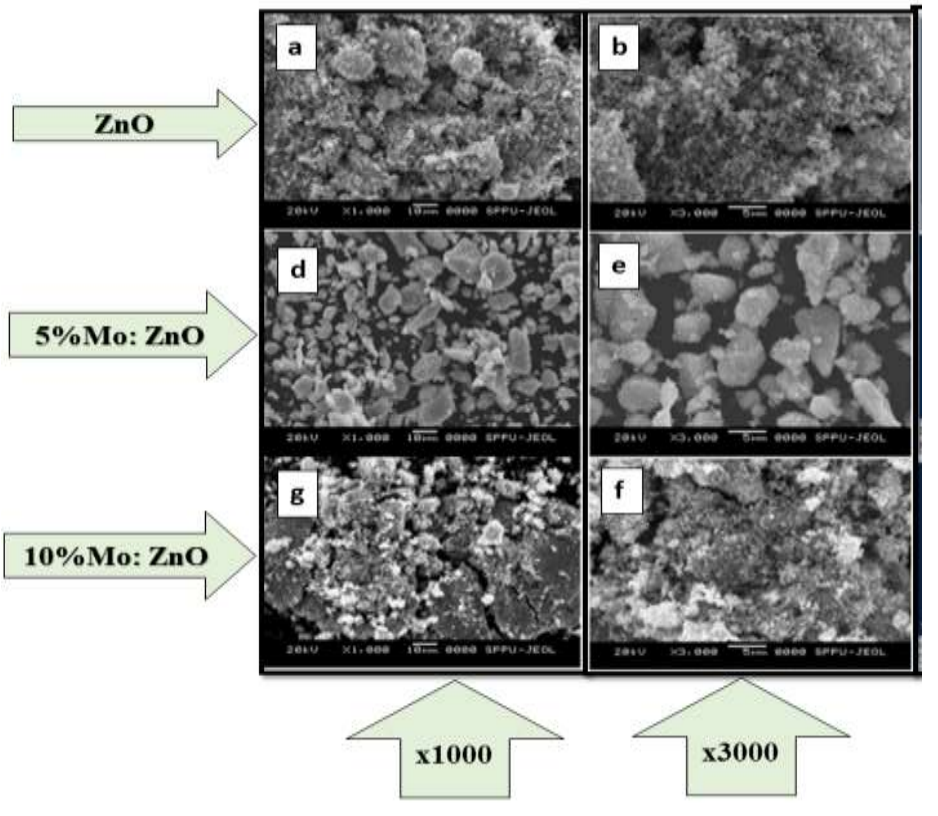

Fig. 4 SEM images of pure, 5% and 10% Mo-doped ZnO nanoparticles at 1K and 3K magnification.

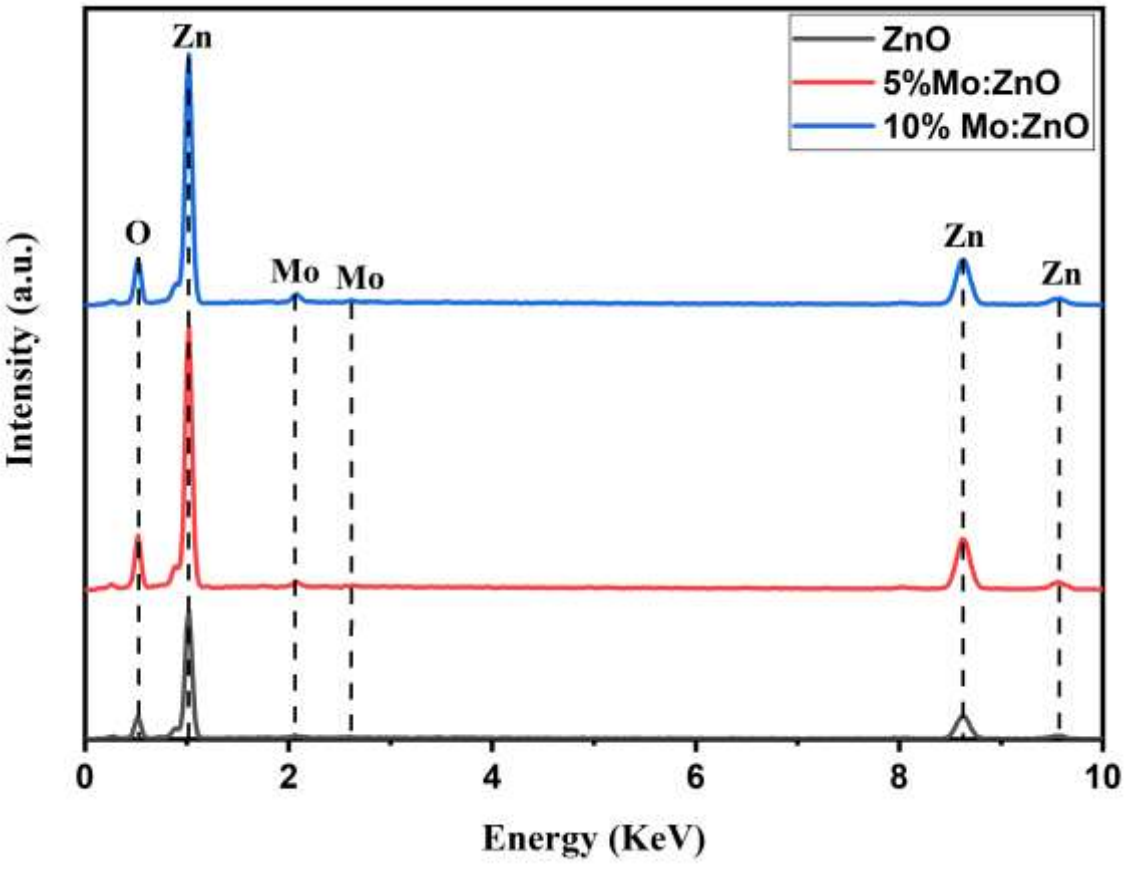

Fig. 5 Elemental composition of pure, 5% and 10% Mo-doped ZnO nanoparticles.

the EDS spectra of all ZnO samples prepared with Zinc acetate precursor. The ZnO matrix shows the distribution of Zn peak and O peak in the matrix, which confirms the purity of ZnO nanoparticles. The presence of the Mo peak in the EDS array indicates the doping of the ZnO with molybdenum. The table displays the atomic weight (wt%) of ZnO and Mo-doped ZnO. Another observation recorded is that the atomic weight percentage in catalysts prepared via zinc acetate precursor is lower than the actual weights used during the synthesis process, which may be caused by a partial amalgamation of molybdenum which was prominently observed for catalysts prepared using zinc acetate precursor. In addition, the observed atomic weight percentage of catalysts prepared by the use of zinc acetate precursors is lower than that of the catalysts used in the synthesis process. This may be due to the partial amalgamation, which was observed to be present in the catalysts prepared by zinc acetate. the elemental composition is tabulated in Table 5.

3.5 Photodegradation study

The photocatalytic activity of zinc oxide (ZnO) and Mo-doped zinc oxide (Mo-ZnO) nanoparticles has been assessed by the use of 50 mg of catalyst loading of 10 ppm dye. Fig. 6 shows UV–visible spectra of Photodegradation of Rose Bengal dye of (a) ZnO, (b) 5%, and (c) 10% Molybdenum doped ZnO powder. This was done by aqueous solutions of Rose Bengal (RB), which was irradiated with UV light at room temperature with a power of 100 mW/cm^2 light intensity. At various time intervals, the absorption spectra of irradiated samples were recorded, and the rate of decolourization of RB was measured in terms of the change in intensity at 464 nm. After 40 minutes of exposure to sunlight (100 mw/cm^2), the absorption band ranging from 350 to 550 nm is 85% lost.

Mo-doped zinc oxide samples demonstrated a higher level of activity than bare zinc oxide, with 5% Mo-doped zinc exhibiting a decrease in the colour of 91%. Furthermore, the addition of 10% Mo to the zinc oxide lattice increased activity, with 79% of the dye's colour being discharged after 30 minutes. The highest activity was achieved when 5% Mo was added to the zinc oxide sample, resulting in a decrease in the dye's colour of 91% within 30 min.

The percentage of degradation efficiencies can be calculated using the Beer-Lambert law, which is illustrated in equation (3).

$$R = \frac{C_0 - C_t}{C_0} \times 100 = \left(\frac{A_0 - A_t}{A_0}\right) \times 100 \qquad (3)$$

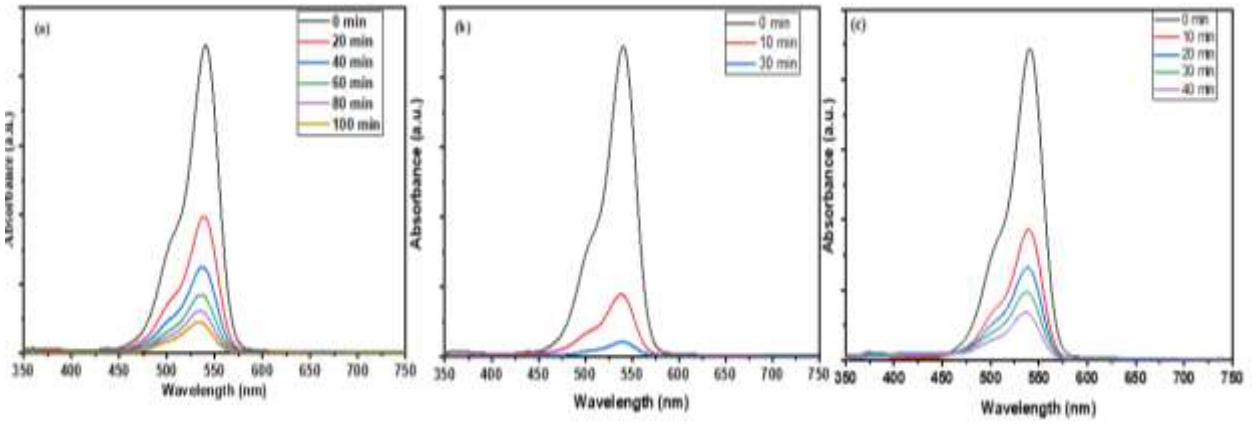

Fig. 6 UV–Visible spectra of Photodegradation of Rose Bengal dye of a) ZnO, b) 5%, c) 10% Molybdenum doped ZnO powder.

Table 5. XRD Rietveld Refinement and EDS Elemental Chemical Composition Parameters of pure, 5% and 10% Mo-doped ZnO nanoparticles.

Parameters		Sample		
		ZnO	5% Mo:ZnO	10% Mo:ZnO
Statistics	R_{wp}	12.03	11.61	12.60
	R_{exp}	13.00	12.35	13.12
	χ^2	0.86	0.88	0.92
	GoF	0.93	0.94	0.96
Crystal structure		Hexagonal Wurtzite	Hexagonal Wurtzite	Hexagonal Wurtzite
Grain Size	(100)	42	50	46
	(002)	57	42	70
	(101)	42	66	53
	Average	47	53	56
a (Å)		3.25	3.26	3.25
c (Å)		5.21	5.21	5.21
Stress ‘e’ (x10-6)		2.9	2.8	2.7
Elemental Chemical Composition (wt%)		Using Rietveld Refinement		
	Zn	80.34	74.92	69.69
	O	19.66	19.30	18.95
	Mo	0.00	5.79	11.36
	Total	100.00	100.00	100.00
		Using Energy Dispersive Spectroscopy (EDS)		
	Zn	64.56	61.37	59.45
	O	35.44	34.42	32.57
	Mo	0.00	4.21	7.98
	Total	100.00	100.00	100.00

where C_0, A_0 is the concentration at an absorbance of the dye in reaction at the time (0) and C_t, A_t is the concentration at an absorbance of the dye after the time (t) minute, respectively.

We have used the kinematic model below to illustrate the relationship between the deterioration of dye over time.

$$Rate = -\frac{dC}{dt} = \frac{kKC}{1+KC} \quad (4)$$

where C is the concentration of dye (mg/L) at an instant ‘t’, t is the time for irradiation of the sample to take place, k is the first order constant of the equation, and K is the absorption constant of dye on nanoparticles. This kinematic model is simplified further to pseudo-first-order equation 5.

$$\ln\frac{C_t}{C_0} = -kt \quad (5)$$

The calculation of half-life $t_{1/2}$ is in equation 6

$$t_{1/2} = \frac{ln2}{k} \quad (6)$$

The Rate constant (k) (mm^{-1}) and Half-life (min) are tabulated in Table 6. The rate constant was assumed to be calculated using a pseudo-first-order kinetic model. The decolorizing profiles obtained corresponded perfectly with the selected model. A straight line was plotted between -ln (C/C_0)

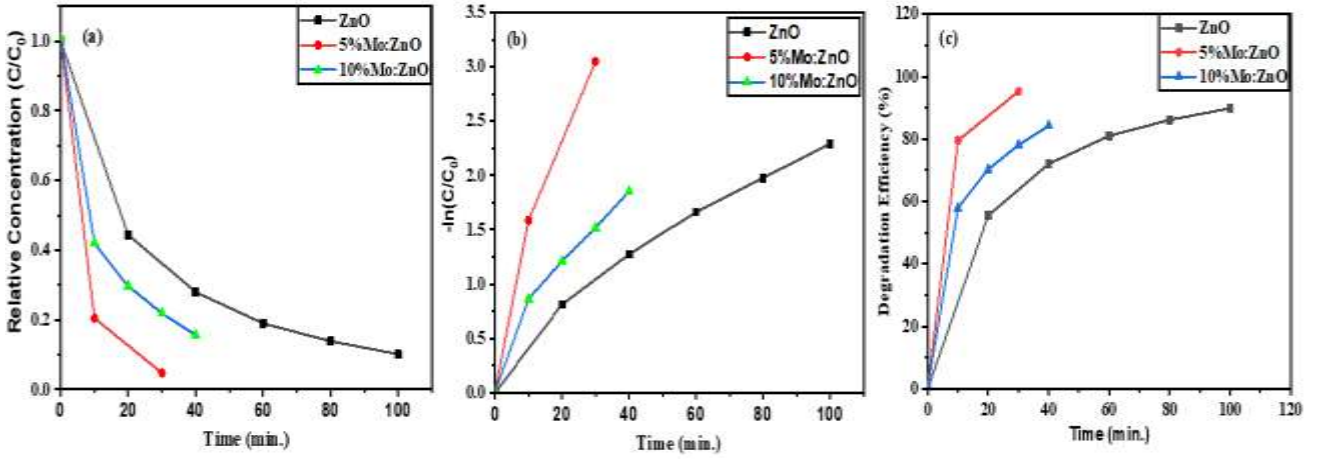

Fig. 7 a) Relative concentration versus irradiation time, b) Plots of - ln (C/Co) versus irradiation time, c) Plots of Photodegradation Efficiency versus irradiation time of pure, 5% and 10% Mo-doped ZnO nanoparticles.

Table 6. Rate constant and half-life calculated by using degradation experiment for samples.

Sample	ZnO	5% Mo: ZnO	10% Mo: ZnO
Rate constant (k) (mm^{-1})	0.06162	0.13133	0.10335
Half-life (min)	11.24928	5.27811	6.70699

and the reaction time, where the slope represented the reaction constant. The prepared samples were also examined under ultraviolet (UV) or visible (VIS) light. The results are shown in Fig. 7.

ZnO doped with an optimum dopant concentration demonstrated significantly higher activity compared to undoped ZnO, as shown in Fig. 7. These results suggest that the local electronic states of this dopant serve as charge carriers traps for photogenic charge carriers under ultraviolet irradiation (UV irradiation). When comparing the activity of doped and undoped zinc oxide samples, the most photodegradable efficiencies were found to be Mo-doped zinc oxide (Mo- ZnO). This suggests that a variety of transition metal ion types offer a different method of trapping charge carriers and prolonging the life of either charge carrier, as the incorporation of a dopant into the zinc oxide matrix may not be in the same position.

4. Mechanism of photo-catalytic reaction

4.1 Mechanism of dye degradation

This study demonstrates the action of ultraviolet light on rose Bengal through the use of a zinc oxide catalyst. During a photodegradation reaction, when zinc oxide is exposed to light with an energy level equal to or greater than its band gap, a valence electron can be attracted to its conduction band, resulting in the formation of a hole in its valence band. These electron–hole pairs that are created by the photogeneration process can either come back together or interact with other molecules on their own. The holes on the valence band react with water on ZnO's surface to make hydroxyl radicals, while the electrons are taken up by adsorbing oxygen to make superoxide radicals.[37] The radical anion then turns into a hydroxyl radical, which is a strong oxidizer, and it attacks the dye molecules to give us the product that's been oxidized. The reaction occurred in this process as follows:[38]

$$ZnO + h\upsilon \rightarrow h^+ + e^- \quad (7)$$

$$h^+ + e^- \rightarrow \text{heat} \quad (8)$$

$$h^+ + H_2O \rightarrow {}^{\bullet}OH + H^+ \quad (9)$$

$$e^- + O_2 \rightarrow O_2^{\bullet -} \quad (10)$$

$$O_2^{\bullet -} + H_2O \rightarrow H_2O_2 \rightarrow 2\,{}^{\bullet}OH \quad (11)$$

$${}^{\bullet}OH + \text{dye} \rightarrow \text{oxidized product} \quad (12)$$

5. Conclusion

The present study demonstrated the synthesis and characterization of zinc oxide (ZnO) and molybdenum Zinc Oxide (Mo: ZnO) as photolytic agents for the oxidation of Rose Bengal. The presence of Mo in Zinc oxide was confirmed through XRD, semi-conductor mass spectrometry, and ultraviolet-vis spectrometry. The XRD results showed the average size of the crystallite and particle size were 27, 22 and 24 nm for three samples respectively. This study highlights changes in average crystallite diameter, variations in ionic radii for zinc and molybdenum, and variations in doping concentration, which contribute to enhanced RB dye abatement under UV irradiation. The photocatalytic activity against RB dyes showed degradation efficiency for ZnO, Mo: ZnO 5%), and Mo: ZnO 10% of 73%, 91%, and 88% in 100 min, 30 min and 40 min respectively, and optimum for 5 wt%

Mo doped ZnO catalyst. The photocatalytic degradation of rose Bengal showed that implantation of 5% Mo significantly enhanced the photocatalytic activity of ZnO.

Acknowledgements

The authors are thankful to the Solar Energy Research and Development (SERD) Department of Science and Technology (DST), Government of India, for financial support through the Major Research project vide Sanction order DST/TMD/CERI/RES/2020/47 (G). Authors gratefully acknowledge Dr. Sachin Desarada from the Computation Department, UNISA, South Africa for assistance with Rietveld refinement of the X-ray diffraction data. Chaitali Jagtap is grateful to Kiran Division, Department of Science and Technology, Government of India, for partial financial support through Women Scientist Scheme-A, vide Sanction order SR/WOS-A/PM-11/2019(G).

Conflict of Interest

There is no conflict of interest.

Supporting Information

Not applicable.

References

[1] M. Afzal, M. Arslan, J. A. Müller, G. Shabir, E. Islam, R. Tahseen, M. Anwar-ul-Haq, A. J. Hashmat, S. Iqbal, Q. M. Khan, Floating treatment wetlands as a suitable option for large-scale wastewater treatment, *Nature Sustainability*, 2019, **2**, 863-871, doi: 10.1038/s41893-019-0350-y.

[2] M. F. Sanad, A. E. Shalan, M. A. Ahmed, M. F. A. Messih, The controlled synthesis and DFT investigation of novel (0D)-(3D) ZnS/SiO_2 heterostructures for photocatalytic applications, *RSC Advances*, 2021, **11**, 22352-22364, doi: 10.1039/d1ra02284a.

[3] B. R. G, R. Dadigala, R. Bandi, K. Seku, K. D, G. Mangatayaru K, A. E. Shalan, Microwave-assisted preparation of a silver nanoparticles/N-doped carbon dots nanocomposite and its application for catalytic reduction of rhodamine B, methyl red and 4-nitrophenol dyes, *RSC Advances*, 2021, **11**, 5139-5148, doi: 10.1039/d0ra10679h.

[4] A. Samir, F. H. Ashour, A. A. Abdel Hakim, M. Bassyouni, Recent advances in biodegradable polymers for sustainable applications, *NPJ Materials Degradation*, 2022, **6**, 68, doi: 10.1038/s41529-022-00277-7.

[5] Y. Zhang, D. Wang, G. Zhang, Photocatalytic degradation of organic contaminants by TiO_2/sepiolite composites prepared at low temperature, *Chemical Engineering Journal*, 2011, **173**, 1-10, doi: 10.1016/j.cej.2010.11.028.

[6] P. E. Lokhande, V. Kadam, C. Jagatap, U. S. Chavan, R. Udayabhaskar, H. M. Pathan, Hierarchical ultrathin nanosheet of $Ni(OH)_2$/rGO composite chemically deposited on Ni foam for NO_x gas sensors, *ES Materials & Manufacturing*, 2022, **17**, 53-56, doi: 10.30919/esmm5e721.

[7] K. Obaideen, N. Shehata, E. T. Sayed, M. Ali Abdelkareem, M. S. Mahmoud, A. G. Olabi, The role of wastewater treatment in achieving sustainable development goals (SDGs) and sustainability guideline, *Energy Nexus*, 2022, **7**, 100112, doi: 10.1016/j.nexus.2022.100112.

[8] D. Pan, S. Ge, J. Tian, Q. Shao, L. Guo, H. Liu, S. Wu, T. Ding, Z. Guo, Research progress in the field of adsorption and catalytic degradation of sewage by hydrotalcite-derived materials. The *Chemical Record*, 2020, **20**, 355-369, doi: 10.1002/tcr.201900046.

[9] K.-D. Balke, Y. Zhu, Natural water purification and water management by artificial groundwater recharge, *Journal of Zhejiang University SCIENCE B*, 2008, **9**, 221-226, doi: 10.1631/jzus.B0710635.

[10] A. M. Hidalgo, M. Gómez, M. D. Murcia, M. Serrano, R. Rodríguez-Schmidt, P. A. Escudero, Behaviour of polysulfone ultrafiltration membrane for dyes removal, *Water Science Technology*, 2018, **77**, 2093-2100, doi: 10.2166/wst.2018.124.

[11] S. Chander, M.-S. Dhaka, Impact of thermal annealing on physical properties of vacuum evaporated polycrystalline CdTe thin films for solar cell applications, *Physica E Low-Dimensional Systems and Nanostructures*, 2016, **80**, 62-68, doi: 10.1016/j.physe.2016.01.012.

[12] M. Goswami, P. Phukan, Enhanced adsorption of cationic dyes using sulfonic acid modified activated carbon, *Journal of Environmental Chemical Engineering*, 2017, **5**, 3508-3517, doi: 10.1016/j.jece.2017.07.016.

[13] M. Jansi Rani, M. Murugan, P. Subramaniam, E. Subramanian, Study of water-soluble dyes adsorption from aqueous solution by Prosopis spicigera L. Wood (PSLW) carbon, *Indian Journal of Chemical Technology*, 2016, **23**, 22-30.

[14] R. W. Gaikwad, S. A. Misal, Sorption studies of methylene blue on silica gel, *International Journal of Chemical Engineering and Applications*, 2010, **1**, 342-345, doi: 10.7763/ijcea.2010.v1.59.

[15] M. Yarahmadi, H. Maleki-Ghaleh, M. E. Mehr, Z. Dargahi, F. Rasouli, M. H. Siadati, Synthesis and characterization of Sr-doped ZnO nanoparticles for photocatalytic applications, *Journal of Alloys and Compounds*, 2021, **853**, 157000, doi: 10.1016/j.jallcom.2020.157000.

[16] S. S. Wagh, V. S. Kadam, C. V. Jagtap, D. B. Salunkhe, R. S. Patil, H. M. Pathan, S. P. Patole, Comparative studies on synthesis, characterization and photocatalytic activity of Ag doped ZnO nanoparticles, *ACS Omega*, 2023, **8**, 7779-7790, doi: 10.1021/acsomega.2c07499.

[17] S. S. Wagh, C. V. Jagtap, V. S. Kadam, S. F. Shaikh, M. Ubaidullah, B. Pandit, D. B. Salunkhe, R. S. Patil, Silver doped ZnO nanoparticles synthesized for photocatalysis application, *ES Energy & Environment*, 2022, **17**, 94-105, doi: 10.30919/esee8e720.

[18] R. Saleh, N. F. Djaja, Transition-metal-doped ZnO nanoparticles: synthesis, characterization and photocatalytic activity under UV light, *Spectrochimica Acta Part A: Molecular Spectroscopy*, 2014, **130**, 581-590, doi: 10.1016/j.saa.2014.03.089.

[19] A.E. Shalan, A.S. Hamdy Makhlouf, S. Lanceros-Méndez, eds, Advances in Nanocomposite Materials for Environmental and Energy Harvesting Applications. Cham: Springer International Publishing, 2022, doi: 10.1007/978-3-030-94319-6.

[20] J. Reguera, F. Zheng, A. E. Shalan, E. Lizundia, Upcycling discarded cellulosic surgical masks into catalytically active freestanding materials, *Cellulose*, 2022, **29**, 2223-2240, doi: 10.1007/s10570-022-04441-9.

[21] A. Al-Shihabi Al-Ani, B. Tokay, W. Zhu, G. Z. Chen, Enhancement of photoconversion efficiency and light harvesting ability of TiO_2 nanotube-arrays with Cu_2ZnSnS_4, *International Journal of Hydrogen Energy*, 2022, **47**, 31003-31013, doi: 10.1016/j.ijhydene.2021.10.110.

[22] S. Gao, J. Zhang, W. Li, S. Jiao, Y. Nie, H. Fan, Z. Zeng, Q. Yu, J. Wang, X. Zhang, Near room temperature and large-area synthesis of ZnO/Cu_2O heterojunction for photocatalytic properties, *Chemical Physics Letters*, 2018, **692**, 14-18, doi: 10.1016/j.cplett.2017.11.062.

[23] G. Murugadoss, Synthesis and characterization of transition metals doped ZnO nanorods, *Journal of Materials Science & Technology*, 2012, **28**, 587-593, doi: 10.1016/s1005-0302(12)60102-9.

[24] V. Ganesh, M. S. A. Hussien, U. P. Shaik, R. Ade, M. I. Mohammed, T. H. AlAbdulaal, H. Y. Zahran, I. S. Yahia, M. S. Abdel-wahab, Impact of Mo-doping on the structural, optical, and electrocatalytic degradation of ZnO nanoparticles: novel approach, *Crystals*, 2022, **12**, 1239, doi: 10.3390/cryst12091239.

[25] A. Khataee, R. Darvishi Cheshmeh Soltani, Y. Hanifehpour, M. Safarpour, H. Gholipour Ranjbar, S. W. Joo, Synthesis and characterization of dysprosium-doped ZnO nanoparticles for photocatalysis of a textile dye under visible light irradiation, *Industrial & Engineering Chemistry Research*, 2014, **53**, 1924-1932, doi: 10.1021/ie402743u.

[26] K. Qi, X. Xing, A. Zada, M. Li, Q. Wang, S.-Y. Liu, H. Lin, G. Wang, Transition metal doped ZnO nanoparticles with enhanced photocatalytic and antibacterial performances: experimental and DFT studies, *Ceramics International*, 2020, **46**, 1494-1502, doi: 10.1016/j.ceramint.2019.09.116.

[27] C. Jagtap, R. Kapale, P. More, V. Kadam, A. Al-Ahmed, T. Alshahrani, F. Khan, Chemical synthesis of pristine and tin-doped ZnO for rose Bengal photocatalytic application, *Journal of Materials Science: Materials in Electronics*, 2023, **34**, 1770, doi: 10.1007/s10854-023-11148-5.

[28] A. A. Shah, M. Ali Bhatti, A. Tahira, A. D. Chandio, I. A. Channa, A. G. Sahito, E. Chalangar, M. Willander, O. Nur, Z. H. Ibupoto, Facile synthesis of copper doped ZnO nanorods for the efficient photo degradation of methylene blue and methyl orange, *Ceramics International*, 2020, **46**, 9997-10005, doi: 10.1016/j.ceramint.2019.12.024.

[29] K. S. Al-Namshah, M. Shkir, F. A. Ibrahim, M. S. Hamdy, Auto combustion synthesis and characterization of Co doped ZnO nanoparticles with boosted photocatalytic performance, *Physica B: Condensed Matter*, 2022, **625**, 413459, doi: 10.1016/j.physb.2021.413459.

[30] C. Jagtap, R. Kapale, P. More, V. Kadam, A. Al-Ahmed, T. Alshahrani, F. Khan, Chemical synthesis of pristine and tin-doped ZnO for rose Bengal photocatalytic application, *Journal of Materials Science: Materials in Electronics*, 2023, **34**, 1770, doi: 10.1007/s10854-023-11148-5.

[31] C. V. Jagtap, V. S. Kadam, T. T. Ghogare, Y. A. Inamdar, A. A. Shaikh, R. S. Mane, A. V. Shaikh, Pristine and cadmium-doped zinc oxide: chemical synthesis and characterizations, *Journal of Materials Science: Materials in Electronics*, 2016, **27**, 12335-12339, doi: 10.1007/s10854-016-5624-9.

[32] C. Jagtap, V. Kadam, S. Jadkar, S. Patole, H. Pathan, Improvement in photovoltaic performance of dye-sensitized solar cell using ruthenium as dopant into titania, *Journal of Materials Science: Materials in Electronics*, 2023, **34**, 1935, doi: 10.1007/s10854-023-11308-7.

[33] S. V. Desarada, K. B. Chavan, N. B. Chaure, Effect of different annealing techniques on CIGS deposited using one-step single-target sputtering, *Journal of Electronic Materials*, 2023, **52**, 3413-3419, doi: 10.1007/s11664-023-10308-x.

[34] S. Patole, M. Islam, R. C. Aiyer, S. Mahamuni, Optical studies of ZnO/Ag nanojunctions, *Journal of Materials Science*, 2006, **41**, 5602-5607, doi: 10.1007/s10853-006-0296-0.

[35] S. Rasouli, S. J. Moeen, Combustion synthesis of Co-doped zinc oxide nanoparticles using mixture of citric acid–glycine fuels, *Journal of Alloys and Compounds*, 2011, **509**, 1915-1919, doi: 10.1016/j.jallcom.2010.10.087.

[36] I. Khan, K. Saeed, I. Khan, Nanoparticles: properties, applications and toxicities, *Arabian Journal of Chemistry*, 2019, **12**, 908-931, doi: 10.1016/j.arabjc.2017.05.011.

[37] J. Kaur, S. Singhal, Heterogeneous photocatalytic degradation of rose Bengal: effect of operational parameters, *Physica B Condensed Matter*, 2014, **450**, 49-53, doi: 10.1016/j.physb.2014.05.069.

[38] P. Amornpitoksuk, S. Suwanboon, S. Sangkanu, A. Sukhoom,

N. Muensit, Morphology, photocatalytic and antibacterial activities of radial spherical ZnO nanorods controlled with a diblock copolymer, *Superlattices and Microstructures*, 2012, **51**, 103-113, doi: 10.1016/j.spmi.2011.11.002.

